The 8th European Congress on Computational Methods in Applied Sciences and Engineering
ECCOMAS Congress 2022
5–9 June 2022, Oslo, Norway

A NEW PROJECTION METHOD FOR NAVIER-STOKES EQUATIONS BY USING RAVIART-THOMAS FINITE ELEMENT

G. Barbi[1*], A. Cervone[2], A. Chierici[3], V. Giovacchini[1], S. Manservisi[1], R. Scardovelli[1] and L. Sirotti[1]

[1] University of Bologna - DIN, Via dei Colli 16, 40136 Bologna (BO), Italy
[2] ENEA FSN-SICNUC-SIN, Via dei Martiri di Monte Sole 4, 40129 Bologna (BO), Italy
[3] Department of Mathematics and Statistics, Texas Tech University, Lubbock, TX 79409, USA
*e-mail: giacomo.barbi3@unibo.it

Key words: Navier-Stokes equations, projection methods, Raviart-Thomas finite elements

Abstract. *Computational Fluid Dynamics codes usually adopt velocity-pressure splitting to reduce the computational effort in the solution of the Navier-Stokes equations. In standard projection methods, the finite element approximations show difficulties to find a solution with discrete free-divergence velocity field in all space points. In this work, a new velocity-pressure method for Navier-Stokes equations that projects the velocity field inside the discrete free-divergence velocity space is presented. This algorithm computes the velocity field on the discrete free-divergence space by using Raviart-Thomas finite elements. The projection is obtained by the minimization of the distance, over the discrete free-divergence space, between the auxiliary field and the desired Raviart-Thomas interpolation space. The Raviart-Thomas discretization is based on the quadrilateral and hexahedral finite element space and therefore the divergence mimetic computational approach is used to avoid the well-known degradation of the divergence term convergence. The auxiliary velocity field is obtained by solving the velocity-pressure split system used in the classical Chorin–Temam algorithm. The pressure is recovered by the orthogonal space to the projection on the Raviart-Thomas interpolation space. The method is investigated with an explicit and semi-implicit treatment of the pressure terms. The issues on boundary conditions and the errors in the reproducibility of the tangential components are investigated. Several numerical examples are reported to support this new projection method.*

1 INTRODUCTION

The simulation of incompressible flows often involves the use of CFD codes. In this context, the divergence-free fields play a key role in the conservation of mass. The most routinely used commercial codes include finite element (FEM) and finite volume (FVM) methods for the approximation of the solution. These two methods are very popular and can be used in different engineering applications with similar costs. The finite volume method is preferred, in some cases, due to the conservation of mass issues that can arise by using the finite element method. However, the desired divergence-free field in all the points of the discrete domain is very hard to obtain for both methods.

In this paper, we deal with the issue of obtaining a FEM solution for the Navier-Stokes system that has a divergence-free velocity field over the discrete domain by using Raviart-Thomas basis functions [1]. This problem is studied in the case of coupled and split pressure-velocity formulation. It is well known that the solution of the coupled incompressible Navier-Stokes system is very CPU expensive and this has led to the development of different numerical algorithms for the treatment of the split system solving the velocity and the pressure fields [2]. Another obstacle to the solution of the Navier-Stokes equations is the coupling between velocity and pressure by the incompressibility constraint that leads to saddle-point matrices in the discrete form. To overcome these problems, Chorin and Temam introduced the projection method by which the Navier-Stokes system is split into two separate steps, one for the resolution of the velocity field and one for the pressure field [3, 4]. This numerical method leads to very efficient simulations and reduces the computational effort. For this reason, several projection methods have been developed in recent years [5].

2 ORTHOGONAL DECOMPOSITION OF VELOCITY FIELD

Unless otherwise specified, we assume in this section that Ω is a bounded subset with appropriate regular boundary $\partial\Omega$. It is well known that a generic function $\mathbf{u} \in \mathbf{L}^2(\Omega)$ can be decomposed as

$$\mathbf{u} = \nabla q + \nabla \times \boldsymbol{\phi}\,, \tag{1}$$

where $q \in H^1(\Omega)/\mathbb{R}$ and $\boldsymbol{\phi} \in \mathbf{H}^1(\Omega)$. We can introduce the divergence space $\mathbf{H}(div, \Omega)$ by

$$\mathbf{H}(div, \Omega) = \{\mathbf{u} \in \mathbf{L}^2(\Omega) : \nabla \cdot \mathbf{u} \in L^2(\Omega)\}\,, \tag{2}$$

and its subspaces $\mathbf{H}_0(div, \Omega)$ and $\mathbf{S}_0(\Omega)$ as

$$\mathbf{H}_0(div, \Omega) = \{\mathbf{u} \in \mathbf{H}(div, \Omega) : \mathbf{u} \cdot \mathbf{n} = 0 \text{ on } \partial\Omega\} \tag{3}$$

and

$$\mathbf{S}_0(\Omega) = \{\mathbf{u} \in \mathbf{H}_0(div, \Omega) : \nabla \cdot \mathbf{u} = 0\}\,, \tag{4}$$

respectively. Because $\mathbf{S}_0(\Omega)$ is a closed subspace of $\mathbf{L}^2(\Omega)$, we have the following decomposition

$$\mathbf{L}^2(\Omega) = \mathbf{S}_0 + \mathbf{S}_0^{\perp}\,, \tag{5}$$

where $(^{\perp})$ denotes the orthogonal of $\mathbf{S}_0$ in $\mathbf{L}^2(\Omega)$ for the standard scalar product.

We are now interested in a decomposition of the velocity field $\mathbf{u}^* \in \mathbf{H}^1(\Omega)$ that satisfy the classical boundary constraint $\int_{\partial\Omega} \mathbf{u}^* \cdot \mathbf{n} = 0$. Now we can introduce divergence-free spaces

$$\mathbf{V} = \{\mathbf{u} \in \mathbf{H}^1(\Omega) : \nabla \cdot \mathbf{u} = 0\}\,, \quad \mathbf{V}_0 = \{\mathbf{u} \in \mathbf{H}_0^1(\Omega) : \nabla \cdot \mathbf{u} = 0\} \tag{6}$$

and decompose $\mathbf{H}^1(\Omega)$ and $\mathbf{H}_0^1(\Omega)$ as

$$\mathbf{H}^1(\Omega) = \mathbf{V} + \mathbf{V}^{\perp}\,, \quad \mathbf{H}_0^1(\Omega) = \mathbf{V}_0 + \mathbf{V}_0^{\perp}\,. \tag{7}$$

It is well known that for each $\mathbf{g} \in \mathbf{H}^{1/2}(\partial\Omega)$ satisfying $\int_{\partial\Omega} \mathbf{g} \cdot \mathbf{n} ds = 0$, there exists a function $\mathbf{u}_0 \in \mathbf{H}^1(\Omega)$ unique up to an additive divergence-free function in $\mathbf{H}_0^1(\Omega)$, such that $\nabla \cdot \mathbf{u}_0 = 0$ in Ω and $\mathbf{u}_0 = \mathbf{g}$ on $\partial\Omega$. Thus, we can consider equally functions in $\mathbf{u}^* \in \mathbf{H}_0^1(\Omega)$ or $\mathbf{u}^* \in \mathbf{H}^1(\Omega)$.

It is possible to formulate the decomposition problem in terms of an optimization problem. Given a function $\mathbf{u}^* \in \mathbf{H}^1(\Omega)$, with $\int_{\partial\Omega} \mathbf{u}^* \cdot \mathbf{n} ds = 0$, we introduce a quadratic functional

$$\mathcal{F}(\mathbf{u}) = \frac{1}{2}\int_\Omega (\mathbf{u} - \mathbf{u}^*)^2 d\Omega \,, \tag{8}$$

with $\mathbf{u} \in \mathbf{H}(div, \Omega)$. We seek $\mathbf{u}$ by minimizing the functional (8) over the space $\mathbf{H}(div, \Omega)$ under the incompressibility constraint

$$\nabla \cdot \mathbf{u} = 0 \,, \tag{9}$$

for all $\mathbf{x} \in \Omega$. The solution of the minimization problem is easy to find by using the Lagrange multiplier method. Given the Lagrange multiplier $p \in L^2(\Omega)$, we set the total variation to zero and obtain

$$\delta\mathcal{L} = \int_\Omega (\mathbf{u} - \mathbf{u}^*)\delta\mathbf{u} d\Omega + \int_\Omega \delta p \nabla \cdot \mathbf{u} d\Omega + \int_\Omega p \nabla \cdot \delta\mathbf{u} d\Omega = 0 \,,$$

for all $\delta\mathbf{u} \in \mathbf{H}(div, \Omega)$ and $\delta p \in L^2(\Omega)$. By setting all the variations to zero we have the following optimality system

$$\int_\Omega \delta p \nabla \cdot \mathbf{u} \, d\Omega = 0 \qquad \forall \delta p \in L^2(\Omega) \,, \tag{10}$$

$$\int_\Omega (\mathbf{u} - \mathbf{u}^*)\delta\mathbf{u} d\Omega + \int_\Omega p \nabla \cdot \delta\mathbf{u} d\Omega = 0 \qquad \forall \delta\mathbf{u} \in \mathbf{H}(div, \Omega) \,. \tag{11}$$

After integration by parts the strong form becomes

$$\nabla \cdot \mathbf{u} = 0 \,, \qquad \mathbf{u}^* = \mathbf{u} - \nabla p \,,$$

with appropriate boundary conditions ($\delta\mathbf{u}|_\Gamma = 0$ or $p|_\Gamma = 0$). Clearly, given $\mathbf{u}^* \in \mathbf{H}^1(\Omega)$, we decompose the field with $\mathbf{u} \in \mathbf{V}$ and $\nabla k \in \mathbf{V}^\perp$. When standard finite element spaces are used,

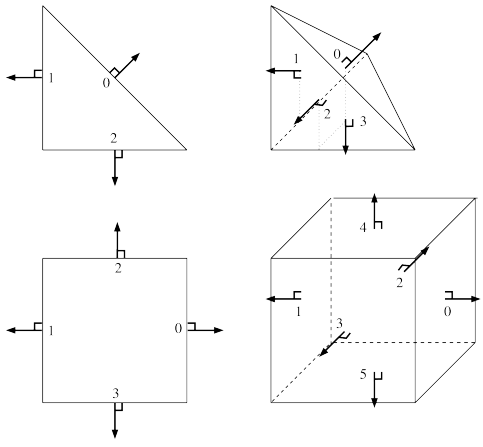

Figure 1: Low order Raviart-Thomas degrees of freedom on different geometries.

the solution of the Navier-Stokes does not belong to the discrete $\mathbf{H}(div, \Omega)$. We use the Raviart-Thomas space to construct this approximation. First, we construct the space over a canonical

element as shown in Figure 1, where low order Raviart-Thomas degrees of freedom on different geometries are symbolically sketched. We suppose that Ω is a polyhedron and that it is covered by a hexahedral or tetrahedral mesh. The mesh consists of elements K characterized by the size h. A single reference element is denoted by $\widehat{K}$ while the real element K is obtained by the application of a trilinear diffeomorphism $F_k : \widehat{K} \to \mathbb{R}^N$ such that $K = F_k(\widehat{K})$, where N is the dimension of the problem. The functions in $\mathbf{H}(div, \Omega)$ are transformed naturally from $\widehat{K}$ to K via Piola transformation tensor $\mathbf{P}$. More precisely, a field $\hat{\mathbf{u}}_h(\widehat{K})$, defined over $\widehat{K}$, can be transformed into $\mathbf{u}_h$ as $\mathbf{u}_h = \mathbf{P}\hat{\mathbf{u}}_h(\widehat{K})$ by

$$\mathbf{u}_h(\mathbf{x}) = detJ(\hat{\mathbf{x}})^{-1} J(\hat{\mathbf{x}}) \hat{\mathbf{u}}_h(\hat{x}) \,, \tag{12}$$

where $\hat{\mathbf{x}} \in \widehat{K}$, $\mathbf{x} = F(\hat{\mathbf{x}})$, and $J(\hat{\mathbf{x}})$ is the Jacobian matrix of the mapping F and $detJ(\hat{\mathbf{x}})$ the determinant of $J(\hat{\mathbf{x}})$.

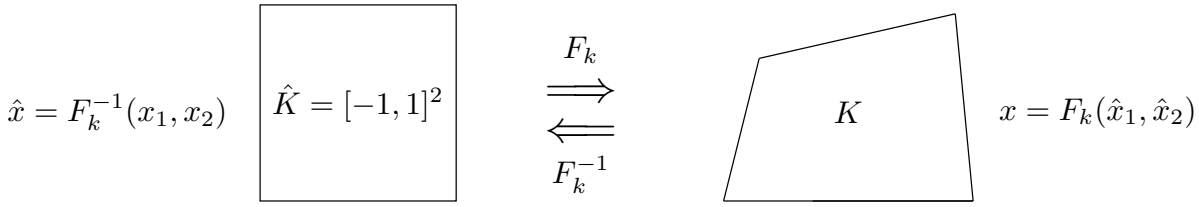

Figure 2: Quadrilateral domain element K and square canonical element $\widehat{K}$.

We remark that the Piola transformation has the following properties

$$\nabla \cdot \mathbf{u}_h(\mathbf{x}) = detJ(\hat{\mathbf{x}})^{-1} \nabla \cdot \hat{\mathbf{u}}_h(\hat{\mathbf{x}}) \quad \forall \hat{\mathbf{x}} \in \widehat{K} \,, \tag{13}$$

$$\int_K \nabla \cdot \mathbf{u}_h(\mathbf{x})\, p_h \, d\mathbf{x} = \int_{\widehat{K}} \nabla \cdot \hat{\mathbf{u}}_h(\hat{\mathbf{x}})\, \hat{p}_h \, d\hat{\mathbf{x}}, \tag{14}$$

$$\int_{\partial K} \mathbf{u}_h(\mathbf{x}) \cdot \mathbf{n}\, p_h \, d\mathbf{x} = \int_{\partial \widehat{K}} \hat{\mathbf{u}}_h(\hat{\mathbf{x}}) \cdot \hat{\mathbf{n}}\, \hat{p}_h \, d\hat{\mathbf{x}} \,, \tag{15}$$

for some $p_h = \hat{p}_h(F^{-1}(\hat{x}))$ while $\mathbf{n}$ and $\hat{\mathbf{n}}$ denote the unit outward normals on K and $\widehat{K}$, respectively. We remark that continuity in the normal direction of the field $\mathbf{u} \cdot \mathbf{n}$ is assured by using the Piola transformation. The construction of a finite element subspace proceeds by assuming all the needed hypotheses on the mesh elements [6].

We construct the Raviart-Thomas finite elements of low order $\mathbf{RT}_0$. The interested reader can refer to [7, 6, 1] for the construction of the $\mathbf{RT}_0$ finite elements. Since our focus is on low-order methods, for the mixed Galerkin method we consider scalar approximations $\hat{p}_h$ on a mesh triangulation τ_h by the piecewise constant function space

$$\widehat{S}_h^0 = \{\hat{p}_h(\hat{\mathbf{x}}) \in L^2(\Omega) | \, \hat{p}_h = c \in \mathbb{R} \quad \forall \hat{\mathbf{x}} \in \widehat{K}, \quad \forall \widehat{K} \in F^{-1}(\tau_h)\} \,. \tag{16}$$

The element triangulation $\hat{\tau}_h$ of canonical elements $\widehat{K}$ is denoted by $F^{-1}(\tau_h)$. The corresponding space based on the domain element K is

$$S_h^0 = \{p_h(\mathbf{x}) \in L^2(\Omega) | \, p_h = \hat{p}_h(F^{-1}(\mathbf{x})) \quad \forall \mathbf{x} \in K, \quad \forall K \in \tau_h\} \,. \tag{17}$$

Clearly, also S_h^0 is a space of piecewise constant functions. For vector fields, we denote by $\widehat{\mathbf{N}}_f$ the basis functions on $\widehat{K}$ on the face denoted by f. In two-dimensional geometries for triangular and quadrilateral meshes, we have $f = 1, \ldots, 3$ and $f = 1, \ldots, 4$, respectively. For three-dimensional geometries, we have $f = 1, \ldots, 4$ and $f = 1, \ldots, 6$ in the case of tetrahedral and hexahedral finite elements, respectively [6, 1]. We define the functional space $\widehat{RT}_0$ generated on $\widehat{K}$ as

$$\widehat{RT}_0 = \{\hat{\mathbf{u}}_h \in \mathbf{H}(div, \Omega) |\, \hat{\mathbf{u}}_h(\hat{\mathbf{x}}) = \sum_f p_f \widehat{\mathbf{N}}_f(\hat{\mathbf{x}}) \quad \forall \hat{\mathbf{x}} \in \widehat{K}, \quad \forall \widehat{K} \in F^{-1}(\tau_h)\}\,, \tag{18}$$

where $p_f = \int_{\partial K} \hat{\mathbf{u}}_h \cdot \hat{\mathbf{n}}_h ds$ is the value of the degree of freedom for the vector field. The degrees of freedom are equal to the number of element faces. The corresponding space is generated as

$$RT_0 = \{\mathbf{u}_h \in \mathbf{H}(div, \Omega) |\, \mathbf{u}_h(\mathbf{x}) = \mathbf{P}\hat{\mathbf{u}}_h(F^{-1}(\mathbf{x})) \quad \forall \mathbf{x} \in K, \quad \forall K \in \tau_h\}\,. \tag{19}$$

Therefore, given $\mathbf{u}_h \in \mathbf{RT}_0 \subset \mathbf{L}^2(\Omega)$ Raviart-Thomas low order, we have

$$\hat{\mathbf{u}}_h(\hat{\mathbf{x}}) = \sum_f p_f \widehat{\mathbf{N}}_f(\hat{\mathbf{x}}) \quad \forall \hat{\mathbf{x}} \in \widehat{K}\,, \quad \mathbf{u}_h(\mathbf{x}) = \sum_f p_f \mathbf{N}_f(\mathbf{x}) \quad \forall \mathbf{x} \in K\,, \tag{20}$$

where p_f are the face fluxes and $\mathbf{N}_f = \mathbf{P}\widehat{\mathbf{N}}_f$ the basis functions for Raviart-Thomas space with $f = 1, \ldots, n_f$. We remark that p_f remains invariant in the transform from the real and the canonical element, due to Piola transformation property (15).

Now we consider the solution of the Navier-Stokes equations. Let $\mathbf{X}_h \subset \mathbf{H}^1(\Omega)$ be a Taylor-Hood finite element space, see for details [8]. Given $\mathbf{u}_h^* \in \mathbf{X}_h$, we want $\mathbf{u}_h \in \mathbf{RT}_0 \subset \mathbf{H}(div, \Omega)$ by minimizing

$$\mathcal{F}(\mathbf{u}_h) = \frac{1}{2}\int_\Omega (\mathbf{u}_h - \mathbf{u}_h^*)^2 d\Omega, \tag{21}$$

$$\nabla \cdot \mathbf{u}_h = 0\,, \tag{22}$$

over the linear function subspace $\mathbf{RT}_0 \subseteq \mathbf{H}(div, \Omega)$. For $\mathbf{u}_h^* \in \mathbf{X}_h \subset \mathbf{H}^1(\Omega)$ Lagrangian quadratic polynomials, we have $\mathbf{u}_h^* = \sum_j \mathbf{u}_{jh}^* \phi_j(\mathbf{x})$ with $\mathbf{u}_{jh}^*$ velocity points and $\phi_j(\mathbf{x})$ basis functions. For $\mathbf{u}_h \in \mathbf{RT}_0 \subset \mathbf{L}^2(\Omega)$ Raviart-Thomas low order, we have $\mathbf{u}_h = \sum_f p_f \mathbf{N}_f(\mathbf{x})$, with p_f flux at faces and $\mathbf{N}_f(\mathbf{x})$ Raviart-Thomas vector basis functions. It is important to remark that the Piola tensor transforms a constant divergence field $\widehat{\nabla} \cdot \hat{\mathbf{u}}_h$ over $\widehat{K}$ into a non-constant divergence field $\nabla \cdot \mathbf{u}_h = detJ^{-1} \widehat{\nabla} \cdot \hat{\mathbf{u}}_h$ over K. This opens a series of issues on the convergence of the divergence for many problems where these basis functions are used. In our case we consider only divergence-free solutions, namely we have $\widehat{\nabla} \cdot \hat{\mathbf{u}}_h(\hat{\mathbf{x}}) = 0$ on all reference elements $\widehat{K}$ and also, from (13) with $detJ^{-1}(\hat{\mathbf{x}}) \neq 0$, $\nabla \cdot \mathbf{u}_h(\mathbf{x}) = 0$ on all real elements K. The interested reader can consult [7, 9]. The minimization of the functional (21), by using the Lagrange multiplier $p_h \in S_h \subset L^2(\Omega)$, gives

$$\begin{aligned} &\int_\Omega \delta p_h \nabla \cdot \mathbf{u}_h \, d\Omega = 0 && \forall \delta p_h \in S_h \subset L^2(\Omega)\,, \\ &\int_\Omega (\mathbf{u}_h - \mathbf{u}_h^*) \cdot \delta \mathbf{u}_h \, d\Omega + \int_\Omega p_h \nabla \cdot \delta \mathbf{u}_h \, d\Omega = 0 && \forall \delta \mathbf{u}_h \in \mathbf{RT}_0(\Omega)\,. \end{aligned} \tag{23}$$

3 NUMERICAL TEST FOR THE MINIMIZATION PROBLEM

In this section, the numerical results related to the presented orthogonal decomposition of the velocity are shown. In particular, we aim to decompose a vector field by following the Helmholtz theorem. In this context, we can introduce a generic velocity field $\mathbf{u}^* \in \mathbf{H}^1(\Omega)$, written as the sum of a gradient and a free-divergence field. Our purpose is to find a velocity $\mathbf{u}_h \in \mathbf{RT}_0$ that corresponds to the known free divergence vector. Several cases have been evaluated, differing by geometry and boundary conditions. The computations are performed by using FEMuS code [10].

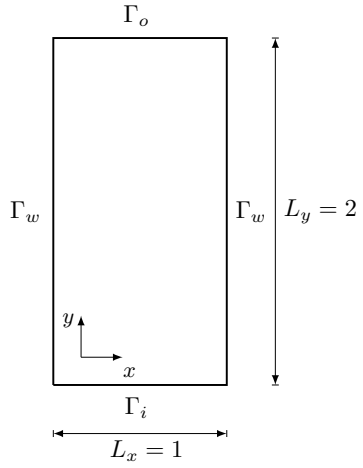

l	n_p	$\|\mathbf{u}_0 - \mathbf{u}_h\|_0$	$\|p_0 - p_h\|_0$	conv. rate
2	2.56E+02	0.4850	0.0093	
3	1.02E+03	0.2435	0.0040	0.9975
4	4.10E+03	0.1217	0.0019	0.9981
5	1.64E+04	0.0609	0.0010	0.9984
6	6.55E+04	0.0305	0.0005	0.9997
7	2.62E+05	0.0152	0.0002	1.0000
8	1.05E+06	0.0076	0.0001	1.0000

Figure 3: Plane channel. Geometry (left), error data and convergence rate (right) for different levels l and mesh points n_p.

Field in a plane channel. In this test, we consider a plane channel geometry, as shown in Figure 3 on the left, and an analytical vector field $\mathbf{u}^* = (u^*, v^*)$. We consider

$$u^* = \frac{\pi}{2}\sin^2(\pi x)\sin(\pi y) + \Big(x - \frac{1}{2}\Big)\Big(\frac{y^2 - 2y}{2}\Big), \tag{24}$$

$$v^* = -\pi \sin^2\Big(\pi\frac{y}{2}\Big)\sin(2\pi x) + \Big(y - \frac{1}{2}\Big)\Big(\frac{x^2 - 2x}{2}\Big). \tag{25}$$

Clearly this vector field $\mathbf{u}^*$ can be decomposed as $\mathbf{u}^* = \mathbf{u}_0 + \mathbf{u}_0^\perp$ with $\mathbf{u}_0 \in \mathbf{V}_0$ and $\mathbf{u}_0^\perp \in \mathbf{V}_0^\perp$ where

$$\mathbf{u}^* = \begin{bmatrix} u^* \\ v^* \end{bmatrix} = \begin{bmatrix} \frac{\pi}{2}\sin^2(\pi x)\sin(\pi y) \\ -\pi\sin^2(\pi\frac{y}{2})\sin(2\pi x) \end{bmatrix} + \begin{bmatrix} (x - \frac{1}{2})\left(\frac{y(y-2)}{2}\right) \\ (y - \frac{1}{2})\left(\frac{x(x-2)}{2}\right) \end{bmatrix} = \mathbf{u}_0 + \mathbf{u}_0^\perp . \tag{26}$$

In this decomposition, defining $p_0 = xy(x-2)y(y-2)/4$, we have $\mathbf{u}_0^\perp = \nabla p_0 = \Big((x - \frac{1}{2})(\frac{y(y-2)}{2}),$ $(y - \frac{1}{2})(\frac{x(x-2)}{2})\Big)$. We compute $(\mathbf{u}_h, p_h)$ by solving system (23). The boundary conditions are

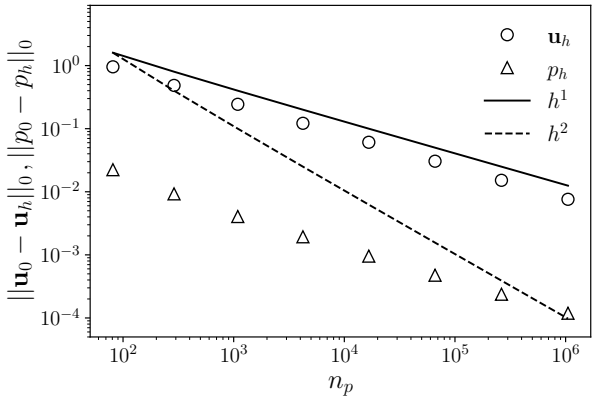

Figure 4: Plane channel case: error convergence.

$\mathbf{u}^* \cdot \mathbf{n} = \mathbf{u}_h \cdot \mathbf{n} = 0$ on $\Gamma_w \cup \Gamma_o$ and $p_0 = p_h = 0$ on Γ_i in order to fix the constant on p_h. The tables on Figure 3 (right) and Figure 4 show the error data and the estimated convergence rate for different refinements (level l with n_p mesh points). The error ϵ_l is defined as the sum of L^2 norm of velocity and pressure error at the level l. Taking the logarithm of the ratio between ϵ_l and ϵ_{l+1} we obtain an estimate of the convergence order, which is reported in the last column. Regarding this value, the results confirm how the order convergence rate follows a linear behavior considering the mesh size h, namely

$$\|\mathbf{u}_0 - \mathbf{u}_h\|_0 \leq Ch\|\mathbf{u}^*\|_1\,, \quad \|p_0 - p_h\|_0 \leq Ch\|p_0\|_1\,. \tag{27}$$

Figure 4 shows the L^2 norm error of velocity and pressure concerning the number of points in the grid. As noted in the previous table, we can notice a good agreement with the linear trend of the error norm represented by the solid black line.

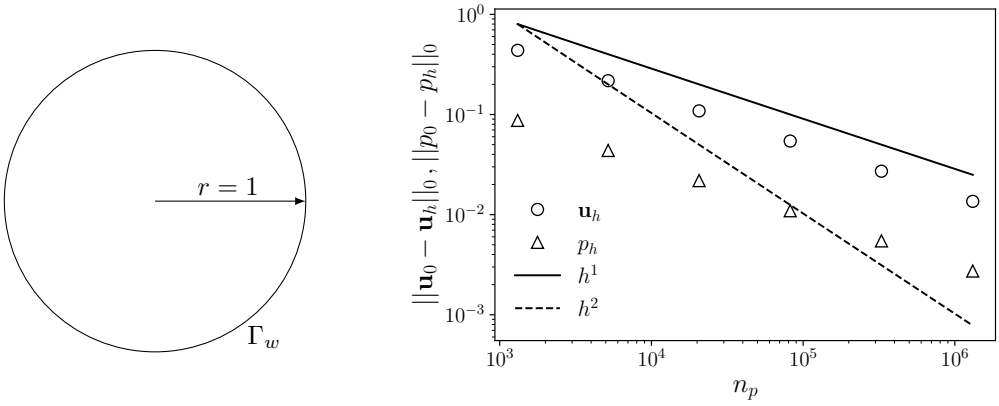

Figure 5: Circle geometry (left) and error convergence (right).

Field in a circle. In this test, we consider a circle, as shown in Figure 5 on the right, and an analytical vector field $\mathbf{u}^* = (u^*, v^*)$, decomposed as $\mathbf{u}^* = \mathbf{u}_0 + \mathbf{u}_0^\perp$, with $\mathbf{u}_0 \in \mathbf{V}_0$ and $\mathbf{u}_0^\perp \in \mathbf{V}_0^\perp$

where

$$\mathbf{u}^* = \begin{bmatrix} u^* \\ v^* \end{bmatrix} = \begin{bmatrix} 4(x^2+y^2-1)y \\ -4(x^2+y^2-1)x \end{bmatrix} + \begin{bmatrix} (x+1)^2 \\ 0 \end{bmatrix} = \mathbf{u}_0 + \mathbf{u}_0^\perp . \tag{28}$$

By setting $p_0 = (x+1)^3/3$, we have $\mathbf{u}_0^\perp = \nabla p_0$. We solve (23) for the $\mathbf{RT}_0$ finite element solution $(\mathbf{u}_h, p_h)$. The boundary conditions are $\mathbf{u}_0 \cdot \mathbf{n} = \mathbf{u}_h \cdot \mathbf{n} = 0$ on Γ_w and $p_0 = p_h = 0$ at the point $\mathbf{x} = (-1, 0)$, needed to fix the constant on p_h. In Figure 5 on the left, the circular geometry is shown, where non-affine quadrilateral elements must be used. The decomposition shows good results and the velocity and pressure error scale linearly with the mesh size h as shown in the table in Figure 5 on the right.

Three-dimensional field. We now consider a three-dimensional field. The domain is shown in Figure 6 on the left. Let us consider the following analytical vector field $\mathbf{u}^* = (u^*, v^*)$.

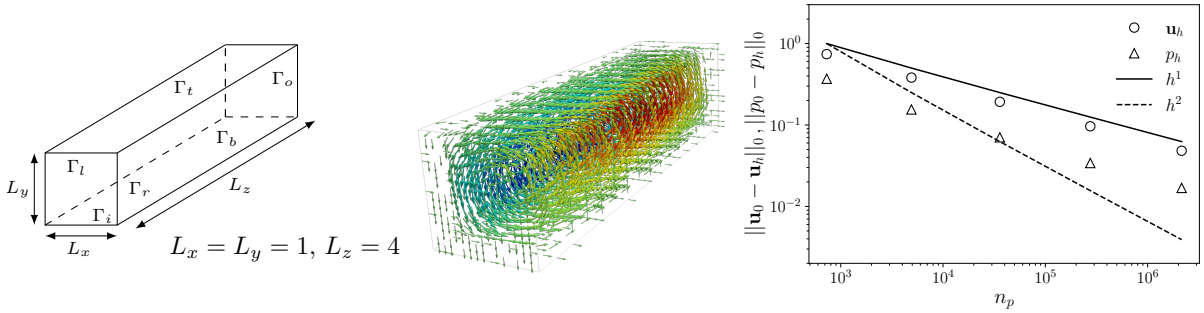

Figure 6: Three-dimensional field: channel geometry (left), field (center) and error as a function of the resolution (right).

$$\begin{bmatrix} u^* \\ v^* \\ \\ w^* \end{bmatrix} = \begin{bmatrix} 2\pi \sin^2(\pi x)\sin(\pi y)\cos(\pi y) z(4-z) \\ -2\pi \sin^2(\pi y)\sin(\pi x)\cos(\pi x) z(4-z) \\ +\pi \sin^2(\pi y)\sin(\pi z/4)\cos(\pi z/4) x(1-x) \\ -4\pi \sin^2(\pi z/4)\sin(\pi y)\cos(\pi y) x(1-x) \end{bmatrix} + \begin{bmatrix} 50(x-0.5)(y^2-y) \\ 50(x^2-x)(y-0.5) \\ \\ 0 \end{bmatrix} . \tag{29}$$

The field, as shown in Figure 6 (center), can be decomposed as $\mathbf{u}^* = \mathbf{u}_0 + \mathbf{u}_0^\perp$ with $\mathbf{u}_0 \in \mathbf{V}_0$ and $\mathbf{u}_0^\perp \in \mathbf{V}_0^\perp$. By setting $p_0 = 25(x^2-x)(y^2-y)$ we have $\mathbf{u}_0^\perp = \nabla p_0$. The (23) is used to solve $(\mathbf{u}_h, p_h) \in \mathbf{RT}_0 \times S_h^0$. The boundary conditions are $\mathbf{u}^* \cdot \mathbf{n} = \mathbf{u}_h \cdot \mathbf{n} = 0$ on boundary and $p_0 = p_h = 0$ at the point $\mathbf{x} = (0, 0, 0)$ needed to fix the constant on p_h. The error between $\mathbf{u}_h$ and $\mathbf{u}_0$ is reported in Figure 6 (right) as a function of the level resolution, namely the number of mesh points n_p. Convergence of first order is guaranteed in both velocity and pressure cases.

4 VELOCITY-PRESSURE SPLIT FOR NAVIER-STOKES EQUATIONS

Considering a generic incompressible fluid flow, with constant physical properties, the pressure and velocity fields can be computed by solving the following Navier-Stokes system

$$\begin{aligned} \frac{\partial \mathbf{u}}{\partial t} + (\mathbf{u}\cdot\nabla)\mathbf{u} &= -\nabla p + \nu\nabla^2\mathbf{u} + \mathbf{f}\,, \\ \nabla\cdot\mathbf{u} &= 0\,. \end{aligned} \tag{30}$$

The solution of the coupled velocity-pressure system (30) is very CPU expensive and this has led to the development of different numerical algorithms for the treatment of the split system for velocity and the pressure fields. In order to overcome these problems, many authors introduced the projection method by which the Navier-Stokes system is split in two separate steps, one for the velocity and one for the pressure [3, 4]. This numerical method leads to an efficient simulation and reduces the computational effort. The interested reader can consult [5] for an overview over projection methods.

To introduce the pressure-velocity split, we discretize the equation by the simple Euler scheme on time. We introduce a fictitious velocity field $\mathbf{u}^{n*}$ and we have

$$\frac{\mathbf{u}^{n*}-\mathbf{u}^{n*}}{\Delta t} + \frac{\mathbf{u}^{n}-\mathbf{u}^{n-1}}{\Delta t} + (\mathbf{u}^{n}\cdot\nabla)\mathbf{u}^{n} = -\nabla p^{n} + \nu\nabla^2\mathbf{u}^{n} + \mathbf{f}\,. \tag{31}$$

Considering $p^n = p^{n-1} + \delta p^n$, we can now split the equation

$$\frac{\mathbf{u}^{n}-\mathbf{u}^{n*}}{\Delta t} = -\nabla\delta p^{n}\,, \tag{32}$$

$$\frac{\mathbf{u}^{n*}-\mathbf{u}^{n-1}}{\Delta t} = -(\mathbf{u}^{n}\cdot\nabla)\mathbf{u}^{n} - \nabla p^{n-1} + \nu\nabla^2\mathbf{u}^{n} + \mathbf{f}\,. \tag{33}$$

There are different approaches for the solution of the pressure-velocity split. The classical pressure-velocity split with incremental algorithm solves a standard Laplacian operator for pressure. By using $\nabla\cdot\mathbf{u}^n = 0$ the pressure equation becomes [5]

$$\nabla\cdot\mathbf{u}^{n*} = \Delta t\nabla^2\delta p^{n}\,, \tag{34}$$

where $\mathbf{u}^{n*}\in\mathbf{H}^1(\Omega)$, $p^n\in H^1(\Omega)$ and $\mathbf{u}^n = \mathbf{u}^{n*} - \nabla\delta p^n \in \mathbf{H}(div,\Omega)$. The Laplacian operator needs boundary conditions for pressure and this may be a problem where velocity boundary conditions are applied in the coupled equation system. In this case one usually sets $\partial p/\partial n|_\Gamma = 0$ which is a non-physical Neumann boundary condition.

In this paper we propose a new velocity-pressure split which consists of the velocity equation

$$\frac{\mathbf{u}^{n*}-\mathbf{u}^{n-1}}{\Delta t} = -(\mathbf{u}^{n*}\cdot\nabla)\mathbf{u}^{n*} - \nabla p^{n-1} + \nu\nabla^2\mathbf{u}^{n*} + \mathbf{f}\,, \tag{35}$$

and the pressure equation

$$\mathbf{u}^{n} - \mathbf{u}^{n*} + \Delta t\nabla\delta p^{n} = 0\,. \tag{36}$$

In this paper we use the Raviart-Thomas optimality problem for solving (36). Considering $k_h = \delta p_h \in S_h \subset L^2(\Omega)$, $\mathbf{u}_h^n \in \mathbf{RT}_0 \subset \mathbf{H}(div, \Omega)$, and $\nabla \cdot \mathbf{u}_h^n = 0$, we have

$$\int_\Omega \delta k_h \nabla \cdot \mathbf{u}_h^n \, d\Omega = 0 \qquad \forall \delta k_h \in S_h \subset L^2(\Omega)\,, \tag{37}$$

$$\int_\Omega (\mathbf{u}_h^n - \mathbf{u}_h^{*n}) \delta \mathbf{u}_h^n \, d\Omega + \int_\Omega k_h \nabla \cdot \delta \mathbf{u}_h^n \, d\Omega = 0 \qquad \forall \delta \mathbf{u}_h^n \in \mathbf{RT}_0(\Omega)\,. \tag{38}$$

5 NUMERICAL RESULTS FOR THE RT_0 PROJECTION METHOD

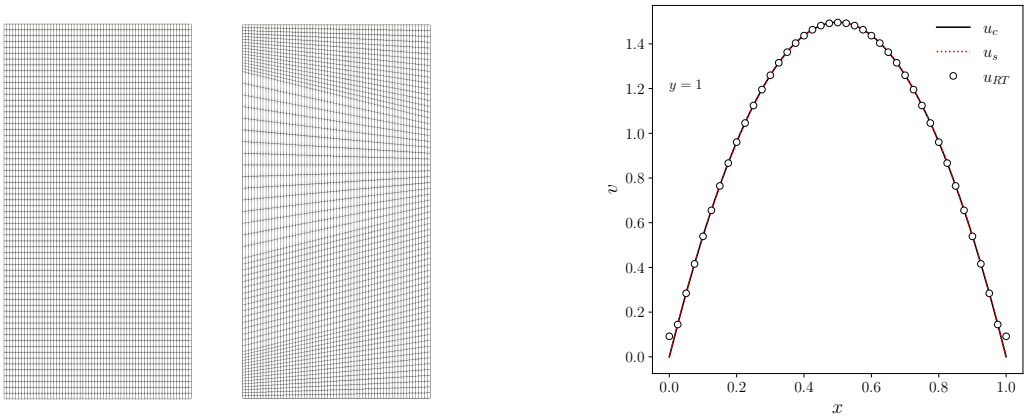

Figure 7: Two-dimensional Poiseuille flow. Regular and irregular mesh for the channel flow (left) and velocity v for coupled, split system and Raviart-Thomas approximation (right).

Two-dimensional Poiseuille flow. In this section, the results of the projection method for the Navier-Stokes equations are reported for standard laminar velocity profile inside a channel, and therefore we expect to obtain the classical Poiseuille parabolic flow.

In Figure 7 (left) the investigated geometries are reported, with particular attention to the irregular mesh with non-affine elements. In Figure 7 (right) the velocity profile for the stream-wise component is reported. In particular, the same field is represented for different numerical solutions: the first one in the solid black line is obtained with a coupled algorithm for the Navier-Stokes equations, the second one in the red dotted line is obtained with a standard split algorithm, and finally the circular markers represent the velocity profile obtained with a split algorithm using the Raviart-Thomas approximation. The plot shows a perfect agreement of the velocity profile computed with the different algorithms.

Two-dimensional cavity. In order to check the convergence error rate, we consider a plane channel flow with wall boundaries, i.e., a cavity configuration. The steady exact Navier-Stokes solution has been imposed on the right-hand side, allowing for the computation of the L^2 norm

l	n_p	$\|\mathbf{u}-\mathbf{u}_h\|_0^2=\epsilon_l^2$	$\frac{\epsilon_l}{\epsilon_{l+1}}$	$\log_2\left(\frac{\epsilon_l}{\epsilon_{l+1}}\right)$
2	2.56E+02	0.23581	-	-
3	1.02E+03	0.05933	1.9936	0.997
4	4.10E+03	0.01487	1.9957	0.998
5	1.64E+04	0.00371	1.9977	0.998
6	6.55E+04	0.00092	1.9996	0.999
7	2.62E+05	0.00023	2.0000	1.000

Table 1: Two-dimensional cavity. Error for steady state $\mathbf{u}_h$ for the $\mathbf{RT}_0$ split approximation.

of the velocity error. We report the exact solution of the velocity components

$$\mathbf{u}^* = \begin{bmatrix} u \\ v \end{bmatrix} = \begin{bmatrix} \frac{\pi}{2}\sin^2(\pi x)\sin(\pi\frac{y}{2})\cos(\pi\frac{y}{2}) \\ -\pi\sin^2(\pi\frac{y}{2})\sin(\pi x)\cos(\pi x) \end{bmatrix}. \tag{39}$$

In Table 1 the error and the order of convergence for different levels of refinement are reported. The last column confirms, also in this case, the linear trend in error convergence for the velocity norm.

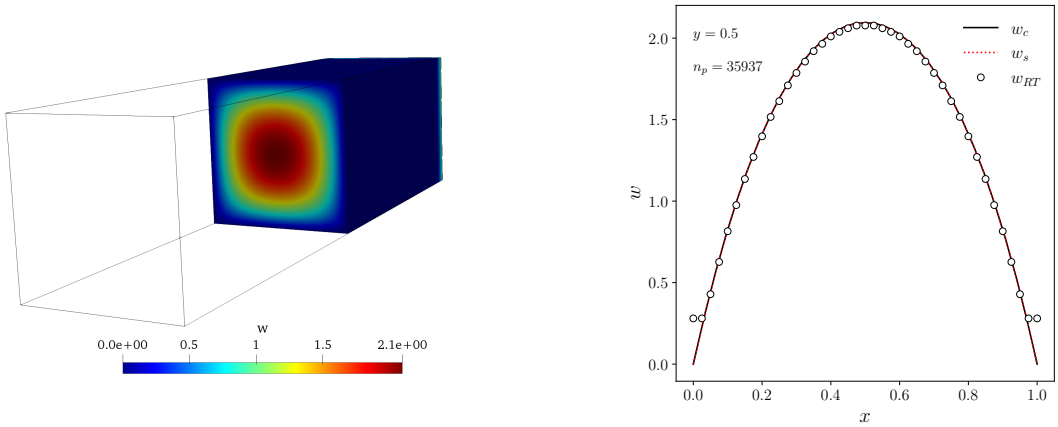

Figure 8: Three-dimensional channel flow. Clip of the w-component of the steady velocity field (right) and its values for coupled Navier-Stokes solution, Raviart-Thomas and standard projection split system.

Three-dimensional channel flow. The three-dimensional geometry of the channel flow is reported in Figure 8 (left) ($L_x = 1$, $L_y = 1$ and $L_z = 4$). The flow enters into the bottom (inlet) and exits through the top (outlet). No-slip boundary conditions are applied on the walls. From Figure 8 (right) the accuracy of the computation can be noticed. Indeed, the velocity profile obtained with the Raviart-Thomas basis projection (35)-(36) is equal to the velocity profile obtained with standard coupled (30) and split algorithms (35)-(34).

6 CONCLUSION

In this paper we have studied a vector decomposition by using Raviart-Thomas basis functions in order to approximate the velocity field, solution of the Navier-Stokes equations. This kind of finite element allows us to have exactly zero divergence at each point, which is an important condition for the mass conservation. Several test cases have been presented using regular and irregular mesh, and the results show a good agreement with the theoretical assumption regarding the order convergence rate. Moreover, the $\mathbf{RT}_0$ space has been used to approximate the velocity field in the framework of the velocity-pressure split algorithm. A minimization problem has been solved in order to compute the velocity and pressure fields, avoiding the resolution of the Laplacian equation for pressure. The numerical results confirm the approximation of the velocity with the advantage of having exact free divergence velocity at each point. In addition, this technique reduces the computational effort of the computation owing to fewer dof number.

REFERENCES

[1] P.A. Raviart and J.M. Thomas, *Introduction a l'analyse numerique des equations aux derivees partielles*, Collection Mathématiques appliquées pour la maîtrisesous, Ciarlet et J.-L. Lions editors, Paris, 1988.

[2] S. Turek, *On discrete projection methods for the incompressible Navier-Stokes equations: An algorithmical approach*, Computer Methods in Applied Mechanics and Engineering, 143(3-4), 271-288, 1997.

[3] A.J. Chorin, *Numerical solution of the Navier–Stokes equations*, Math. Comput., 22(104), 745–762, 1968.

[4] R. Temam, *Navier–Stokes Equations: Theory and Numerical Analysis*, North-Holland, Amsterdam, 1984.

[5] J.L. Guermond, P. Minev and Jie Shen, *An overview of projection methods for incompressible flows*, Comput. Methods Appl. Mech. Engrg. 195, 6011–6045, 2006.

[6] R.S. Falk, P. Gatto and P. Monk, *Hexahedral H(div) and H(curl) finite elments*, esaim M2AN, 45, 115–143, 2011.

[7] D. N. Arnold, D. Boffi and S. Richard, *Quadrilateral H(div) finite elements*, SIAM J. Numer. Anal., 42(6), 2429-2451, 2005.

[8] V. Girault and P.A. Raviart, *Finite Element Methods for Navier-Stokes Equations*, Springer-Verlag New York, USA 1986.

[9] P. B. Bochev and D. Rizdal, *Rehabilitation of the lowest-order Raviart–Thomas element on quadrilateral grids*, SIAM Journal on Numerical Analysis, 47(1), 487-507, 2009.

[10] A. Chierici, G. Barbi, G. Bornia, D. Cerroni, L. Chirco, R. Da Vià, V. Giovacchini, S. Manservisi, R. Scardovelli and A. Cervone, *FEMuS-Platform: a numerical platform for multiscale and multiphysics code coupling*, 9th edition of the International Conference on Computational Methods for Coupled Problems in Science and Engineering, 2021.